Contrasting seasonal fluxes of planktonic foraminifera and impacts on paleothermometry in the Mozambique Channel upstream of the Agulhas Current

Ulrike Fallet,[1] Geert-Jan Brummer,[1] Jens Zinke,[1,2] Sanne Vogels,[1,2] and Herman Ridderinkhof[3]

Received 5 February 2010; revised 9 July 2010; accepted 5 August 2010; published 11 December 2010.

[1] We assess δ^{18}O- and Mg/Ca–based paleothermometry in relation to seasonal variations in the shell fluxes of the surface-dwelling planktonic foraminifera *G. ruber* and *G. trilobus*. Using deep-moored sediment traps in the Mozambique Channel, upstream of the Agulhas Current, we find a distinct antiphase response to the annual cycle in sea surface temperature (SST) in *G. ruber* and *G. trilobus*. Maximum fluxes of *G. ruber* occur in late austral summer (February–March) when SST ranges between 28.7°C and 30.3°C. By contrast, *G. trilobus* maxima appear in early winter (June–July) at a lower SST between 25.3°C and 27.0°C. Cross-correlation of the 2.5 year time series data confirmed that the *G. ruber/G. trilobus* ratio (R/T ratio) closely followed the annual cycle in SST, as did their paired δ^{18}O and Mg/Ca. In all proxies, *G. ruber* showed a 3 week phase lag against SST and *G. trilobus* of 6 weeks consistent with (semi-) lunar population turnover rates in combination with a 1 week settling time to the 2500 m deep ocean floor. After correcting for these lags, we derived five independent equations for improved paleothermometry in the southwestern Indian Ocean that specify flux-weighted annual mean SST. The offset between flux-weighted SST of *G. ruber* and *G. trilobus* and annual mean instrumental SST is about 0.8°C despite their strong seasonality in shell export. This is far less than the mean difference in instrumental SST between summer and winter of 3.2°C. Both species therefore closely reflect annual mean SST in sediments within a margin of +0.5°C for *G. ruber* and –0.3°C for *G. trilobus*. We also find that multiple linear regression of the five proxies (R/T ratio and the δ^{18}O, Mg/Ca of *G. ruber* and *G. trilobus*) strongly reduces the effects of fast rotating eddies and improves the correlation coefficient from an r^2 of 0.4 to an r^2 of 0.8.

Citation: Fallet, U., G.-J. Brummer, J. Zinke, S. Vogels, and H. Ridderinkhof (2010), Contrasting seasonal fluxes of planktonic foraminifera and impacts on paleothermometry in the Mozambique Channel upstream of the Agulhas Current, *Paleoceanography*, *25*, PA4223, doi:10.1029/2010PA001942.

1. Introduction

[2] Foraminiferal tracers fundamentally contribute to our understanding of past ocean and climate systems [*Elderfield*, 2002]. Many paleotemperature reconstructions rely on the analysis of foraminiferal shell chemistry since they record seawater temperature via the changing $^{18}O/^{16}O$ [*Bemis et al.*, 1998; *Emiliani*, 1955; *Shackleton and Vincent*, 1978] and Mg/Ca ratios of their carbonate shell [*Anand et al.*, 2003; *Nürnberg et al.*, 1996]. Model and field studies have shown substantial seasonal differences on foraminiferal shell fluxes [*Deuser et al.*, 1981] that may strongly influence $\delta^{18}O_c$– [*Deuser*, 1987] and Mg/Ca–based paleoreconstructions of annual SST [*Fraile et al.*, 2009]. In order to quantify the effect of such seasonal changes on paleothermometry, we deployed time series sediment traps in the deep Mozambique Channel [*de Ruijter et al.*, 2005] which is characterized by a mean 3.2°C seasonality in SST. For that purpose we examined a 2.5 year time series for two common surface-dwelling species of planktonic foraminifera, symbiont-bearing *G. ruber* and *G. trilobus* in terms of their shell flux, δ^{18}O and Mg/Ca. Both species are widely used in paleothermometry because they occur frequently throughout the (sub-) tropical surface oceans [*Bé and Hutson*, 1977], are well known from culture studies [*Bé*, 1980; *Bé et al.*, 1981] and persist during Quaternary climate change [*Emiliani*, 1955; *Emiliani and Shackleton*, 1974; *Peeters et al.*, 2004]. Here we develop equations relating *G. ruber* and *G. trilobus* shell fluxes, $\delta^{18}O_c$ and Mg/Ca to remote sensing SST of the upstream Agulhas Current.

[3] Both *G. ruber* and *G. trilobus* are important constituents of the tropical fauna in the SW Indian Ocean. This specific tropical fauna can be transported to the Agulhas Current via the Mozambique Channel leaving a record of Agulhas Leakage in the adjacent Atlantic [*Peeters et al.*, 2004]. Satellite altimetry has shown that instead of a con-

[1] Department of Marine Geology, Royal NIOZ, Den Burg, Netherlands.
[2] Fakulteit der Aard- en Levenswetenschappen, Vrije Universiteit Amsterdam, Amsterdam, Netherlands.
[3] Department of Physical Oceanography, Royal NIOZ, Den Burg, Netherlands.

0883-8305/10/2010PA001942

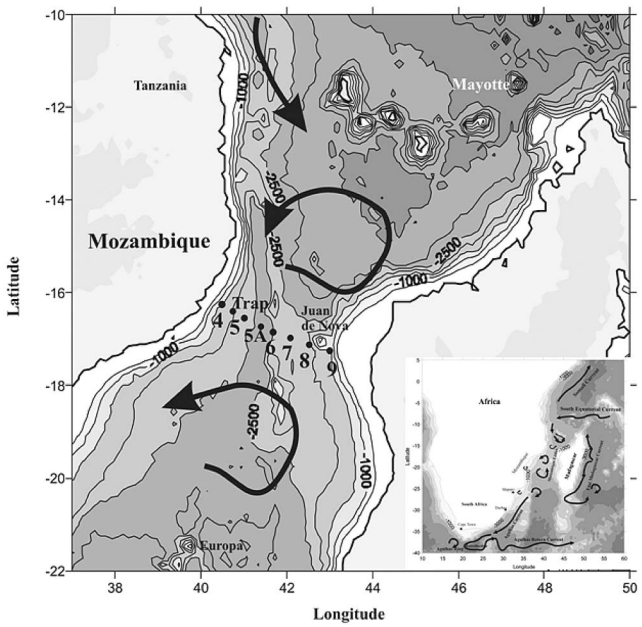

Figure 1. Study area with trap and CTD locations. Channel depth is given in 500 m isobars. Inset shows the greater Agulhas Current system with prevailing eddy migration pathways.

tinuous Western boundary current we find poleward transport by fast rotating, mesoscale eddies through the Mozambique Channel which can exceed 300 km in diameter [*Schouten et al.*, 2003]. These eddies are responsible for the about 17 Sv poleward transport of tropical waters [*van der Werf et al.*, 2010] thereby contributing to the combined 35 Sv transport of the Agulhas Current. Indeed, they are responsible for the formation and shedding of Agulhas Rings into the South Atlantic [*de Ruijter et al.*, 1999]. Yet, they also cause large-scale perturbations at their margin that may affect temperature calibrations we aim to define for the Mozambique Channel. Cross-correlation is used to identify specific lags in the proxy temperatures with respect to satellite SST before applying reduced major axis regression to derive the first temperature calibrations for the SW Indian Ocean.

2. Material and Methods

[4] In order to trace seasonal temperature in planktonic foraminifera we monitored settling particle fluxes using deep-moored sediment traps deployed upstream of the modern Agulhas Current (Figure 1). Associated with the Long-term Ocean Climate Observation (LOCO) program [*de Ruijter et al.*, 2005; *de Ruijter et al.*, 2006; *Palastanga et al.*, 2006] we deployed two consecutive time series sediment trap moorings in the central Mozambique Channel from November 2003 to March 2006 (Figure 1). Each time the Technicap PPS 5 sediment trap with a baffled collecting area of 1 m^2 and a 24-cup automated sampling carousel was positioned at 250 m above the channel floor at 2250 m water depth. Prior to deployments, sample cups were filled with a $HgCl_2$ poisoned and borax-buffered solution of seawater collected from the deployment depth [*Lončarić et al.*, 2007]. The sediment traps were programmed to a 3 week sampling interval for a 2.5 year period on the same site (Table 1). Samples were wet-split using a binary Folsom splitter with a precision of >95% [*Lončarić et al.*, 2007; *Sell and Evans*, 1982]. Aliquots were processed by sequential wet oxidation in hot alkaline H_2O_2 to extract and clean the foraminiferal shells [*Fallet et al.*, 2009].

[5] Shells from the surface-dwelling species *G. ruber* (white) and *G. trilobus* were analyzed for shell flux, weight and paired $\delta^{18}O_c$ and Mg/Ca (Table 1). In order to minimize a potentially large error in $\delta^{18}O$ and Mg/Ca associated with the lumping of different morphotypes [*Steinke et al.*, 2005], we used only *G. ruber* sensu stricto that was by far the most common with all sensu lato types being rare (less than 5%). For the same reasons, we analyzed only *G. trilobus* (Reuss, 1850) in this study excluding *G. sacculifer* (Brady, 1879) with its final sac-like chamber, a terminal morphotype [*Brummer et al.*, 1987] with a deeper depth habitat [*Bijma and Hemleben*, 1994; *Erez and Honjo*, 1981]. All analyses were performed on specimens from the narrow 250–315 μm fraction to minimize any size effects on shell chemistry [*Kroon and Darling*, 1995; *Peeters et al.*, 1999] and because both species are most abundant in this particular size fraction. Additional counts of *G. ruber* and *G. trilobus* specimens in the >150 μm fraction confirmed that size-related changes do not interfere with the species ratio found for the 250–315 μm fraction.

[6] All $\delta^{18}O$ analyses on foraminiferal shells were done on a Thermo Finnigan MAT253 with Kiel IV device with a precision of <0.1‰. Shell weights in the 250–315 μm fraction ranged between 10–16 μg for *G. ruber* and 13–20 μg for *G. trilobus* (Table 1). If available we isolated a minimum of 20 specimens per sample which were gently crushed to open their chambers as well as to homogenize the material. An aliquot of 10 to 20 μg of cleaned carbonate was weighed and subsequently measured for $\delta^{18}O_c$ against the NBS19 standard. All samples were analyzed in duplicate (Table 1) with a standard deviation of 0.05‰. In addition, seawater samples collected in March 2008 by CTD-Rosette profiling across the Mozambique Channel were analyzed in duplicate for $\delta^{18}O_w$ on a Thermo Finnigan Delta + mass spectrometer equipped with a GASBENCH-II preparation device. Between 0.5 and 1 ml of water sample is injected through the septum cap of a 10 ml exetainer vial filled with a mixture of helium and 0.2% CO_2. The oxygen in the headspace CO_2 is allowed to isotopically equilibrate with the water sample for 24 h at a temperature of 22°C. Subsequently the CO_2-helium gas mixture is transported to the GASBENCH-II by use of a helium flow through a flushing needle system. In the GASBENCH-II, water is extracted from the gas, by use of NAFION tubing, and CO_2 is analyzed in the mass spectrometer after separation of other gases in a GC column. Values are reported as $\delta^{18}O$ against V-SMOW. The long-term reproducibility of a routinely analyzed lab water standard is better than 0.1‰.

[7] Foraminiferal tests not used for $\delta^{18}O$ analyses were cleaned according to the protocol of *Barker et al.* [2003] to

Table 1. Time Series Shell Flux and Weights of *G. ruber* and *G. trilobus* and Their Paired $\delta^{18}O$ and Mg/Ca in the 250–315 μm, >150 μm Size Fraction[a]

			G. ruber (250–315 μm)							*G. trilobus* (250–315 μm)						
Sample	Start Date Sampling	SST (°C)	$\delta^{18}O$ (‰)	STD (‰)	Mg/Ca (mmol/mol)	STD (mmol/mol)	Weight (μg)	Shell Fluxes (m^{-2} day^{-1})	>150 μm Shell Fluxes (m^{-2} day^{-1})	$\delta^{18}O$ (‰)	STD (‰)	Mg/Ca (mmol/mol)	STD (mmol/mol)	Weight (μg)	Shell Fluxes (m^{-2} day^{-1})	>150 μm Shell Fluxes (m^{-2} day^{-1})
MOZ1 - A01	23 Nov 2003	28.03	−2.43	0.02	5.68	0.02	-	8.00	-	−2.26	0.01	-	-	-	1.04	-
MOZ1 - A02	14 Dec 2003	28.13	−2.56	0.02	5.51	0.02	-	14.78	-	−2.23	0.01	3.62	0.01	-	2.61	-
MOZ1 - A03	4 Jan 2004	28.69	−2.59	0.04	5.36	0.01	-	10.43	211.58	−2.42	0.02	3.46	0.01	-	2.43	17.67
MOZ1 - A04	25 Jan 2004	28.88	−2.63	0.01	5.86	0.00	10.00	17.74	-	−2.36	0.01	-	-	-	1.91	-
MOZ1 - A05	15 Feb 2004	29.26	−2.48	0.03	5.95	0.01	10.03	50.43	288.15	−2.26	0.02	4.09	0.00	19.95	8.70	36.12
MOZ1 - A06	7 Mar 2004	28.66	−2.48	0.01	5.67	0.02	11.20	119.48	-	−2.67	0.02	4.12	0.00	-	7.30	-
MOZ1 - A07	28 Mar 2004	29.66	−2.31	0.05	5.65	0.01	-	23.65	-	−2.43	0.02	4.32	0.02	-	4.35	-
MOZ1 - A08	18 Apr 2004	29.39	−2.43	0.02	5.61	0.01	14.60	41.57	96.42	−2.55	0.01	4.12	0.01	-	10.96	31.53
MOZ1 - A09	9 May 2004	27.26	−2.09	0.02	5.85	0.02	12.23	49.04	-	−2.30	0.01	3.99	0.00	13.50	21.91	-
MOZ1 - A10	30 May 2004	26.51	−2.42	0.01	5.40	0.01	-	23.83	50.49	−2.36	0.01	3.69	0.01	15.92	22.43	47.58
MOZ1 - A11	20 Jun 2004	25.76	−2.37	0.02	5.24	0.01	-	8.17	-	−2.20	0.01	3.74	0.01	-	13.04	-
MOZ1 - A12	11 July 2004	25.31	−1.69	0.02	4.57	0.01	11.73	17.22	82.74	−2.03	0.02	3.66	0.00	16.30	28.52	84.90
MOZ1 - A13	1 Aug 2004	25.48	−2.39	0.02	-	-	-	2.26	-	−2.08	0.01	3.43	0.01	16.58	8.70	-
MOZ1 - A14	22 Aug 2004	25.06	−1.45	0.02	4.39	0.01	12.56	10.78	-	−1.93	0.01	3.51	0.00	-	6.26	-
MOZ1 - A15	12 Sept 2004	25.48	−1.81	0.01	4.90	0.02	-	14.09	52.94	−1.89	0.01	3.43	0.00	18.75	17.91	52.20
MOZ1 - A16	3 Oct 2004	25.58	−2.12	0.02	4.73	0.00	10.33	34.61	-	−2.11	0.01	3.45	0.01	14.00	18.43	-
MOZ1 - A17	24 Oct 2004	26.88	−1.72	0.02	4.70	0.01	11.63	13.04	-	−2.05	0.02	3.48	0.00	-	6.61	-
MOZ1 - A18	14 Nov 2004	28.19	−2.26	0.01	5.78	0.00	12.15	12.35	129.68	−2.12	0.01	3.62	0.00	20.15	9.04	31.90
MOZ1 - A19	5 Dec 2004	28.46	−2.52	0.02	5.13	0.00	-	7.65	-	−2.18	0.01	-	-	-	1.39	-
MOZ1 - A20	26 Dec 2004	29.24	−2.50	0.02	5.53	0.01	13.63	61.04	-	−2.02	0.02	3.91	0.01	-	6.43	-
MOZ1 - A21	16 Jan 2005	28.94	−2.65	0.01	5.82	0.01	10.53	79.30	271.30	−2.39	0.01	4.14	0.00	-	6.61	12.70
MOZ1 - A22	6 Feb 2005	28.91	−2.31	0.01	6.21	0.00	12.10	40.70	-	−2.40	0.02	4.11	0.00	-	8.35	-
MOZ1 - A23	27 Feb 2005	29.17	−2.33	0.01	4.90	0.01	-	77.22	-	−2.10	0.00	3.97	0.01	16.53	18.20	-
MOZ2 - A01	1 Apr 2005	28.91	−2.87	0.01	4.97	0.01	10.75	101.22	-	−1.81	0.01	3.74	0.00	-	6.26	-
MOZ2 - A02	24 Apr 2005	28.16	−2.73	0.01	5.57	0.01	11.75	73.04	-	−2.12	0.01	3.84	0.01	-	10.43	-
MOZ2 - A03	17 May 2005	27.76	-	-	5.08	0.00	13.40	67.48	-	−2.45	0.02	3.78	0.00	18.15	19.48	-
MOZ2 - A04	9 Jun 2005	27.04	−2.52	0.02	5.16	0.01	16.25	66.43	-	−2.42	0.01	3.90	0.01	16.00	32.00	-
MOZ2 - A05	2 Jul 2005	26.31	−2.51	0.01	4.86	0.01	12.70	15.30	-	−2.32	0.02	3.88	0.02	20.50	31.65	-
MOZ2 - A06	25 Jul 2005	25.70	*−3.06*	*0.04*	4.79	0.01	13.63	25.22	-	−2.09	0.01	3.75	0.01	14.20	24.35	-
MOZ2 - A07	17 Aug 2005	25.45	−2.07	0.02	3.75	0.00	-	10.96	-	−1.66	0.02	3.85	0.01	-	21.04	-
MOZ2 - A08	8 Sep 2005	25.48	−2.25	0.01	3.81	0.01	11.46	25.04	-	−1.92	0.01	3.78	0.00	-	24.87	-
MOZ2 - A09	2 Oct 2005	26.36	−2.46	0.02	4.10	0.01	-	7.65	-	−2.00	0.01	3.33	0.01	16.43	24.35	-
MOZ2 - A10	25 Oct 2005	27.15	−2.19	0.01	4.05	0.01	-	6.26	-	−1.73	0.02	3.28	0.01	-	25.57	-
MOZ2 - A11	17 Nov 2005	27.41	−2.34	0.02	4.66	0.00	14.70	23.13	-	−2.14	0.01	3.39	0.01	19.00	5.91	-
MOZ2 - A12	10 Dec 2005	28.75	−2.36	0.02	4.66	0.00	-	13.57	-	−2.13	0.02	3.54	0.01	16.31	4.00	-
MOZ2 - A13	2 Jan 2006	28.98	−2.60	0.01	5.03	0.01	11.13	43.83	-	−2.16	0.01	3.96	0.00	15.55	4.52	-
MOZ2 - A14	25 Jan 2006	29.43	−2.59	0.01	5.30	0.00	11.55	28.00	-	−2.32	0.01	3.72	0.01	18.03	12.52	-
MOZ2 - A15	17 Feb 2006	29.79	−2.38	0.03	5.16	0.01	12.00	30.78	-	−2.30	0.02	3.83	0.00	-	5.91	-
MOZ2 - A16	12 Mar 2006	30.27	−2.60	0.05	5.20	0.02	11.18	20.52	-	−2.33	0.01	3.96	0.01	-	3.65	-

[a]Data in italics are outliers and are not included in calculations. Missing data are interpolated between the previous and consecutive value.

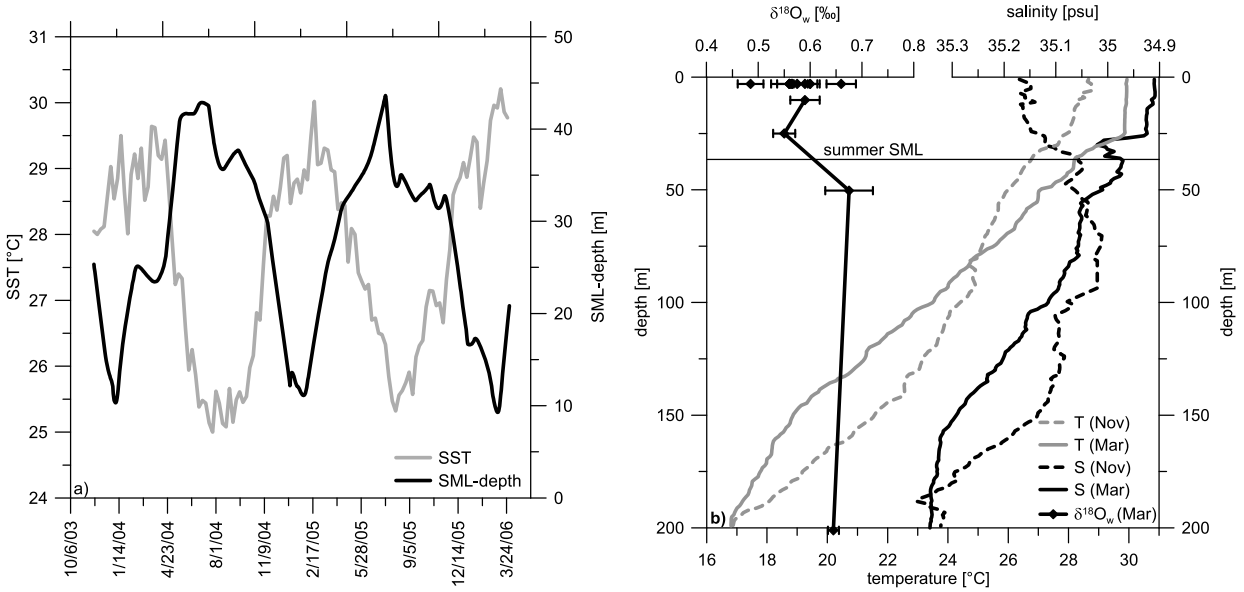

Figure 2. (a) Time series SST and surface-mixed layer depth obtained from satellite remote sensing showing a pronounced antiphase relationship. (b) Temperature-salinity-depth profiles and $\delta^{18}O$ of seawater of at the trap site from the upper 200 m at the mooring station on 23 November 2003 and 3 March 2006. Note the poorly developed surface mixed layer (SML depth indicated with black line) in austral spring (23 November 2003).

remove any adsorbed phases, organic matter and clay minerals and then analyzed for Mg/Ca. Cleaned samples were dissolved in 1000 μl of ultraclean 0.1M HNO_3, and analyzed by high resolution ICP-MS using a Thermo Fischer Scientific Element-2 equipped with a double spray chamber and Teflon microflow nebulizer. Mg/Ca ratios were quantified using the ICP-MS intensity ratio calibration method of *Rosenthal et al.* [1999]. After calcium determination by fast prescanning, samples were diluted to 20 ppm calcium. Analyses of the reference materials BAM RS3 and BAS ECRM 752–1 [*Greaves et al.*, 2005] gave Mg/Ca of 0.786 and 3.737 mmol/mol, respectively, well within the 1σ standard deviation of the calibration mean [*Greaves et al.*, 2008; *Rosenthal et al.*, 2004].

[8] Paired shell fluxes, $\delta^{18}O_c$ and Mg/Ca proxy temperatures of *G. ruber* and *G. trilobus* were contrasted against weekly averaged satellite SST (Figures 2, 3, 4, and 5) from the NOAA database (http://nomad1.ncep.noaa.gov) for the area 16–17°S and 40–41°E, directly above the trap site. The same approach was followed for the surface mixed layer (SML) depth, which was obtained from NASA's Giovanni database (http://gdata1.sci.gsfc.nasa.gov/daac-bin/G3/gui.cgi?instance_id=ocean_model_day) as daily averages. In addition to the remote sensing parameters, we used in situ temperature measurements from shipboard CTD profiling from 23 November 2003 (austral spring) and 3 March 2006 (late summer) across the transect including the actual trap site. We found that satellite SSTs were 0.1°C lower than in situ CTD temperatures at 3 m water depth and we corrected the satellite SST accordingly by adding 0.1°C to each point in the time series.

[9] In order to identify seasonality for the relatively short record of particle fluxes with a comparatively low resolution we cross-correlated all proxies with SST to evaluate the degree of similarity between two waveforms as a function of time. For cross-correlation we used a mixed-effect regression model [*Hedeker and Gibbons*, 1996b] which accounts for dependencies in the data with a nesting structure. Estimation of the parameters involves computing a marginal maximum likelihood solution using both the expectation-maximization algorithm and Fisher scoring [*Hedeker and Gibbons*, 1996a]. After correcting the data set for the specific time lags, SST calibration lines for each individual proxy are determined by reduced major axis regression. Reduced major axis regression is used because both SST and proxy parameters can be considered independent variables. Reduced major axis regression minimizes the triangular area between the data points and the regression line. Residuals of each proxy are plotted against SST to determine whether they contain a significant trend and are *not* Gaussian distributed (Null-Hypothesis). The visual inspection of the residuals was validated by applying the χ^2-test to the residuals. For measured χ^2 values higher than the critical χ^2 of 5.99 we rejected the Null-Hypothesis and conclude that our model describes the bivariate data set well (auxiliary material Figures S1a-S1g).[1]

3. Results

3.1. Seasonal Oceanography

[10] The Mozambique Channel, located between Madagascar and Africa, is governed by the annual migration of the ITCZ between 20°S and 15°N in the tropical southwestern

[1] Auxiliary materials are available in the HTML. doi:10.1029/2010PA001942.

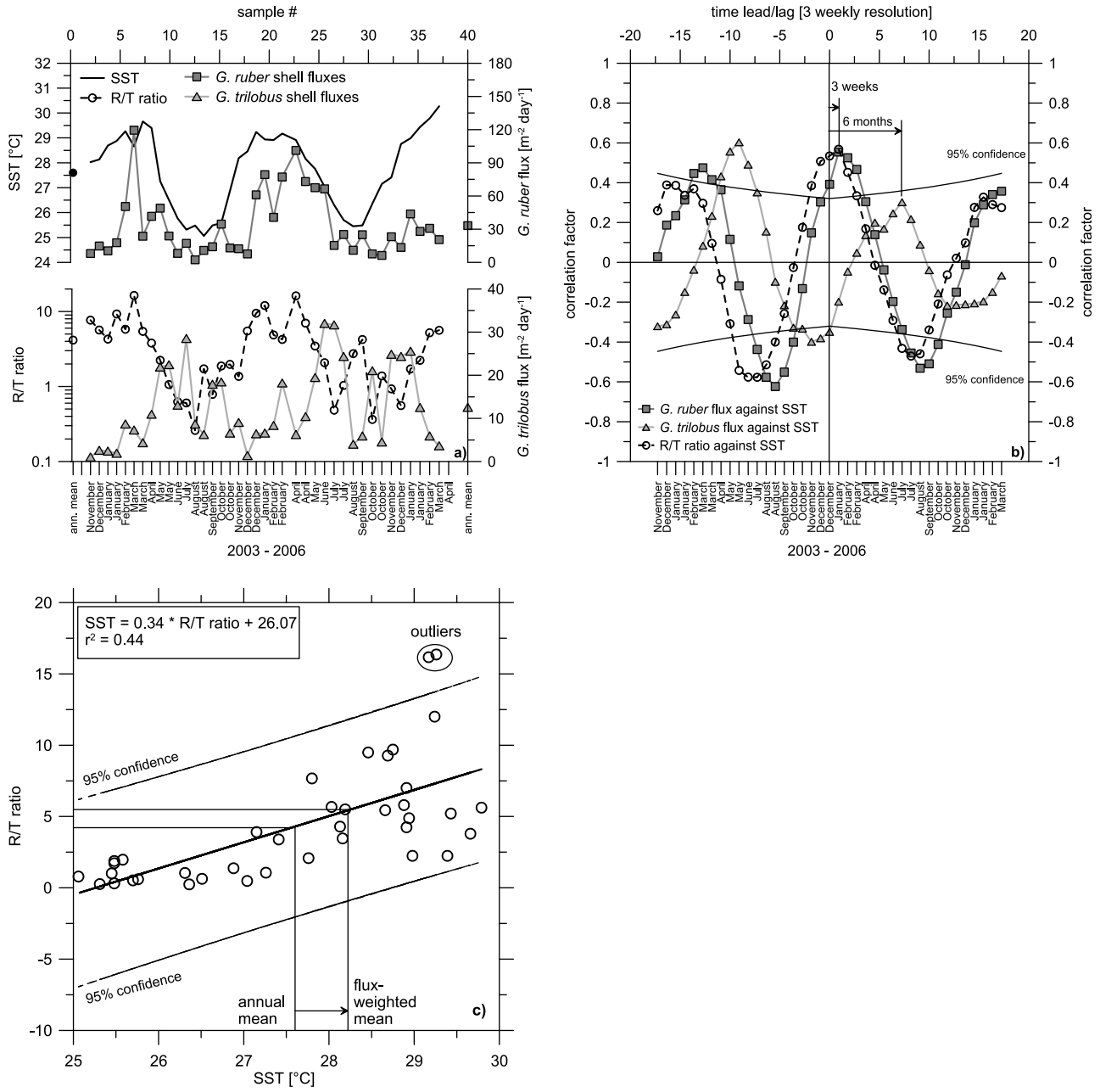

Figure 3. (a) Three-weekly resolved shell fluxes of 2.5 years time series *G. ruber* and *G. trilobus*, their ratio (R/T ratio), and SST. (b) Cross-correlation of *G. ruber* and *G. trilobus* fluxes with SST shows a conspicuous lag of 3 weeks and 6 months, indicating that *G. ruber* predominantly reproduces in summer and *G. trilobus* reproduces in winter months. The R/T ratio also lags SST by 3 weeks when cross-correlated. (c) Reduced major axis regression of lag-corrected R/T ratios against SST. Analysis of the residuals (χ^2 test) returns a χ^2 of 130.97, far above the critical χ^2 of 5.99, indicating that the linear model describes the data well.

Indian Ocean (Figure 1). Associated with the monsoon system, seasonal forcing is expressed in pronounced SST changes from winter minima of 25°C to summer maxima above 30.2°C with an annual mean of 27.6°C (Table 1 and Figure 2a). With the onset of summer in late November increase in rainfall caused by the seasonal migration of the ITCZ slightly lowers sea surface salinities from 35.2 psu in winter to 34.9 psu in summer in the Mozambique Channel (Figure 2b). The Mozambique Channel can be characterized as an oligotrophic region with extremely low concentrations of chlorophyll *a* in surface waters between 0.075 mg/m^3 in summer and 0.25 mg/m^3 in winter. Shipboard CTD profiles

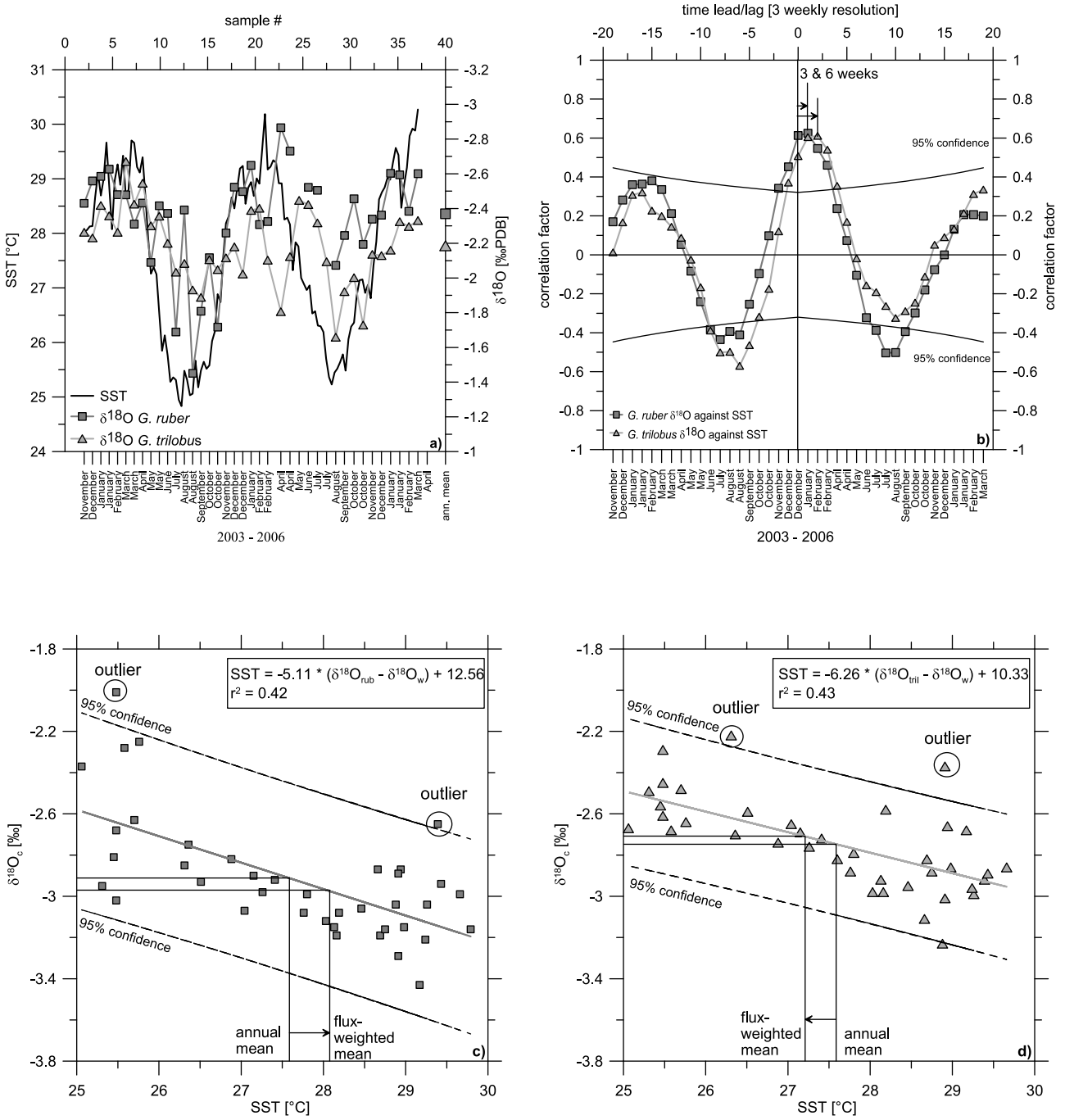

Figure 4. (a) Three-weekly resolved $\delta^{18}O_c$ data of 2.5 years time series *G. ruber* and *G. trilobus* and SST. (b) Cross-correlation of $\delta^{18}O_c$ of *G. ruber* and *G. trilobus* with SST shows a conspicuous lag of 3 and 6 weeks. (c and d) Reduced major axis regression of lag- and $\delta^{18}O_w$-corrected $\delta^{18}O_c$ data against SST. Analysis of the residuals returns χ^2 values of 15.80 for *G. ruber* and 35.45 for *G. trilobus*, far above the critical χ^2 of 5.99. Arrow indicates the shift of flux-weighted proxy SST against annual mean SST derived from satellite data.

indicate a developing SML in spring that reaches to about 10 m water depth which deepens to approximately 30 m by the end of March (Figure 2b). This confirms satellite observations of the SML depth in the Mozambique Channel that indicate a strong seasonality with a deep SML of 40 m during winter and shallow SML of 10 m during summer. Thus, the 25°C winter minimum SST is found at 40 m, the depth of winter mixing.

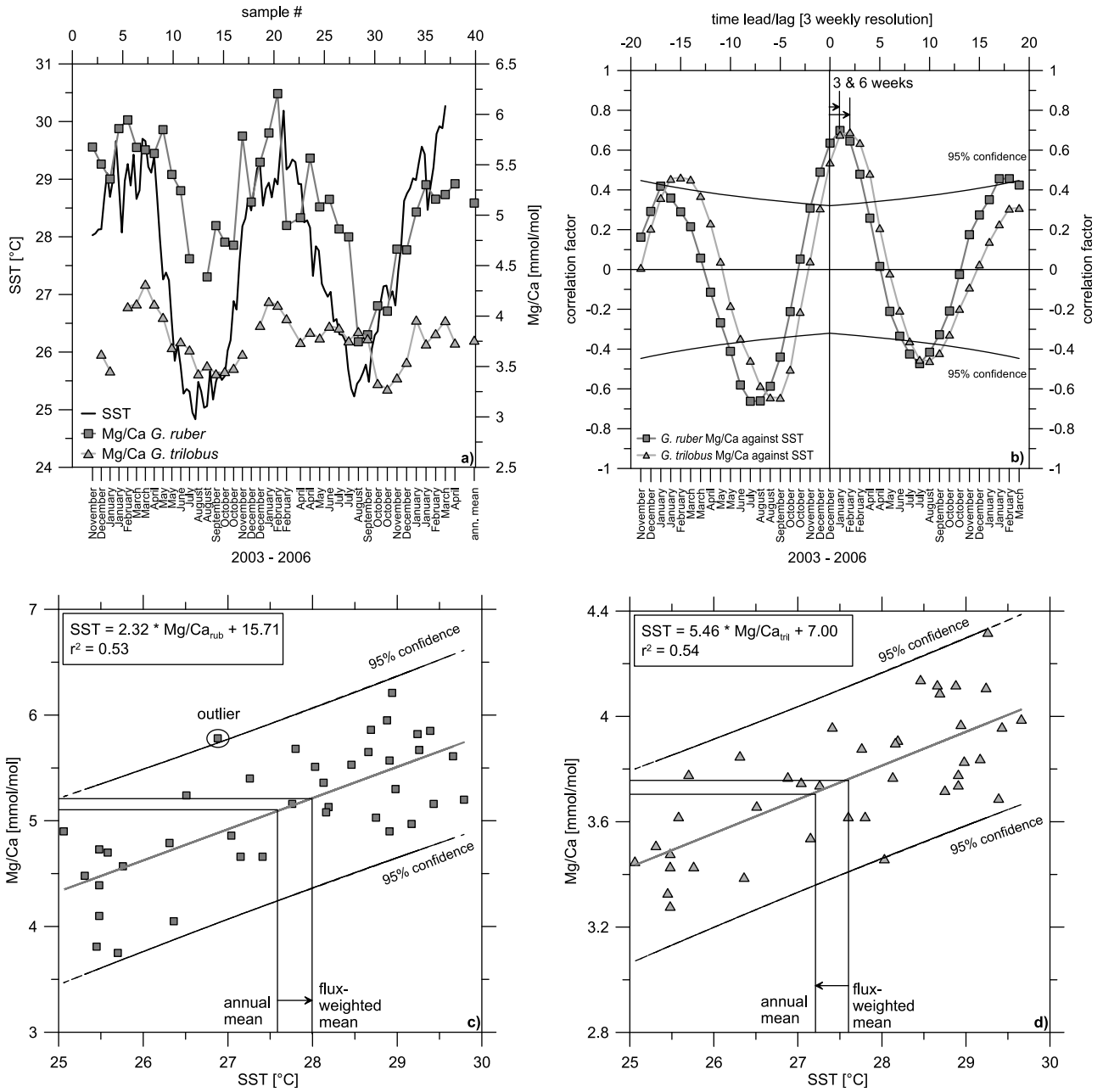

Figure 5. (a) Three-weekly resolved Mg/Ca data of 2.5 years time series *G. ruber* and *G. trilobus* and SST. (b) Cross-correlation of Mg/Ca of *G. ruber* and *G. trilobus* with SST shows a conspicuous lag of 3 and 6 weeks. (c and d) Lag-corrected Mg/Ca data against SST. Analysis of the residuals returns a χ^2 of 10.20 for *G. ruber* and 12.18 for *G. trilobus*, well above the critical χ^2 of 5.99. Arrow indicates the shift of flux-weighted proxy SST against annual mean SST derived from satellite data.

3.2. Antiphase Shell Fluxes

[11] We observed a strong seasonality in *G. ruber* shell fluxes in the 250–315 μm size fraction with a major pulse arriving in February–March and a minor one in October. Shell fluxes of *G. ruber* were highest in late austral summer with maximum values of 100–120 shells m^{-2} day^{-1}, approximately 5 times higher than during the remainder of the year (Table 1 and Figure 3a). Minimum values occurred in winter with 2–8 shells m^{-2} day^{-1} adding up to an annual average of ~25–30 shells m^{-2} day^{-1}. Additionally, we observed that *G. ruber* specimens from the wide >150 μm size fraction follow the seasonality we already observed for the narrow size fraction with maxima during summer and minima during winter (Table 1). Peak fluxes in austral summer (December to early March) accounted for 48% of the annual shell flux of *G. ruber*. *G. ruber* therefore behaves

as a summer species with highest export production in February and March that lags SST by about 3 weeks.

[12] By contrast, *G. trilobus* showed highest shell fluxes in austral winter (May–July) of about 32 shells m^{-2} day^{-1} and minima in summer of 1 shell m^{-2} day^{-1} (Table 1 and Figure 3a) at an annual average of 10 shells m^{-2} day^{-1}. The recurring maximum in *G. trilobus* fluxes during early austral winter (June–July) contributes about 47% to the annual shell flux when low SSTs prevail in response to the migration of the ITCZ. Similarly to the narrow size fraction, we noticed that *G. trilobus* specimens from the wide >150 μm size fraction showed highest fluxes during winter and lowest fluxes during summer months (Table 1). We therefore classify *G. trilobus* as a winter species with peak shell export under low SSTs.

[13] Seasonality is most clearly expressed by the ratio of shell fluxes for *G. ruber* and *G. trilobus* (R/T ratio) which varies in concert with the annual cycle in SST rather than in antiphase, with R/T values ranging from <0.5 at the onset of austral winter to >10 in summer (Figure 3a). Cross-correlation of the 2.5 year time series shows that R/T ratios closely follow seasonal SST with a 3 week lag and has an flux-weighted ratio of 5.44 (Figure 3b). In order to determine seasonal SST from the R/T ratio of time series shell flux, we corrected for the observed 3 week offset before applying reduced major axis regression against SST (Figure 3c). From that we derive

$$\mathrm{SST} = 0.34 * \frac{J_{rub}}{J_{tril}} + 26.07, \quad (1)$$

where J_{rub} is the shell flux of *G. ruber* and J_{tril} that of *G. trilobus* with a correlation coefficient r^2 of 0.44 being statistically significant at the 95% confidence limit. The equation returns proxy SSTs ranging between 26.2°C and 31.6°C at a flux-weighted mean of 28.2°C. To validate whether our model is appropriate for our data set we applied the χ^2 test to the residuals. The measured χ^2 value is 130.97, which is far above the critical χ^2 of 5.99, thus our model describes the bivariate data set very well (Figure S1a). This not only holds for the R/T ratio in the narrow 250–315 μm size range but also for the >150 μm size fraction and emphasizes its sensitivity to seasonal changes in size-frequency distribution of either species. Despite the much larger shell fluxes, the wide R/T ratio is similar to the narrow R/T ratio and also follows seasonal SST with *G. ruber* as a summer and *G. trilobus* as a winter species. Thus, the R/T proxy appears applicable to a wide range of size fractions since the majority of the export production is reflected in both, the narrow and the wide, size range (Figure S2).

3.3. Shell $\delta^{18}O$ and Mg/Ca Thermometry

[14] The $\delta^{18}O_c$ of both *G. ruber* and *G. trilobus* follows the phases in SST on seasonal time scales (Table 1 and Figure 4a). Time series $\delta^{18}O_c$ ranges from −2.9‰ to −1.5‰ PDB with an annual average of −2.35‰ in *G. ruber*, and from −2.7‰ to −1.7‰ with an annual average of −2.18‰ in *G. trilobus* with standard deviations of less than 0.05‰. Since $\delta^{18}O_c$– temperature depends on the $\delta^{18}O_w$ of the ambient seawater we corrected all data by 0.56‰ which is the average $\delta^{18}O_w$ for all analyzed surface samples. Seasonality in $\delta^{18}O_w$ was not observed and values of $\delta^{18}O_w$ vary only slightly between 0.55‰ and 0.68‰ in the upper 200 m at the mooring site and between 0.49‰ and 0.66‰ in surface waters taken across the channel (Figure 2). Cross-correlated with SST we find that *G. ruber* lags maximum SSTs by 3 weeks and *G. trilobus* by 6 weeks (Figure 4b). Corrected for this offset, reduced major axis regression produces

$$\mathrm{SST}_{rub} = -5.11 * \left(\delta^{18}O_{rub} - \delta^{18}O_w\right) + 12.56 \quad (2)$$

$$\mathrm{SST}_{tril} = -6.26 * \left(\delta^{18}O_{tril} - \delta^{18}O_w\right) + 10.33, \quad (3)$$

where $\delta^{18}O_{rub}$ and $\delta^{18}O_{tril}$ are the oxygen isotope composition of the foraminiferal shells and $\delta^{18}O_w$ equals 0.56‰ in the ambient seawater (Figures 4c and 4d). The regressions have correlation coefficients r^2 of 0.42 and 0.43, respectively, which is significant at the 95% confidence interval with χ^2 values of 15.80 and 35.45 for the residuals, both well above the critical χ^2 of 5.99 in our model (Figures S1b and S1c). The equations return proxy SSTs ranging between 23.1°C and 30.2°C for *G. ruber* and between 24.5°C and 30.7°C for *G. trilobus* with flux-weighted SSTs of 28.1°C for *G. ruber* and 27.2°C for *G. trilobus*. Thus, flux-weighted averages for $\delta^{18}O$ yield proxy SSTs that are 0.5°C higher (*G. ruber*) and 0.3°C lower (*G. trilobus*) than annual mean SST of 27.6°C over the 2.5 year period of the trap deployment (Figures 4c and 4d).

[15] Seasonality is even more pronounced in foraminiferal Mg/Ca, with values for *G. ruber* from 3.8 mmol/mol to 6.2 mmol/mol with an annual mean of 5.1 mmol/mol. Those for *G. trilobus* are lower and less variable, ranging between 3.3 mmol/mol and 4.2 mmol/mol with an annual mean of 3.8 mmol/mol (Table 1 and Figure 5a). Cross-correlation of Mg/Ca of both species with SST shows that they behave strongly seasonal like they do in $\delta^{18}O_c$ (Figure 5b) again with a lag of 3 weeks for *G. ruber* and 6 weeks for *G. trilobus*. After correcting for this offset we derive the following reduced major axis regressions (Figures 5c and 5d)

$$\mathrm{SST}_{rub} = 2.32 * \mathrm{Mg/Ca}_{rub} + 15.71 \quad (4)$$

$$\mathrm{SST}_{tril} = 5.46 * \mathrm{Mg/Ca}_{tril} + 7.00, \quad (5)$$

where Mg/Ca is the Mg/Ca composition of the species' shells in the 250–315 μm fraction. The regressions yield a correlation coefficient r^2 of 0.53 and 0.54, respectively, which is significant at the 95% confidence interval. Their residuals return χ^2 values of 10.20 and 12.18, both also above the critical value (Figures S1d and S1e). The application of a linear rather than an exponential model is in contrast to other studies [e.g., *Anand et al.*, 2003; *Nürnberg et al.*, 1996]. However, in this study, we calibrate against a relatively narrow seasonal SST range of 5.2°C which is well described by a linear model. The equations return proxy SSTs between 24.5°C and 30.1°C for *G. ruber* and between 25.0°C and 29.9°C for *G. trilobus* with a flux-weighted mean of 28.0°C for *G. ruber* and 27.3°C for *G. trilobus*. Similar to $\delta^{18}O$, flux-

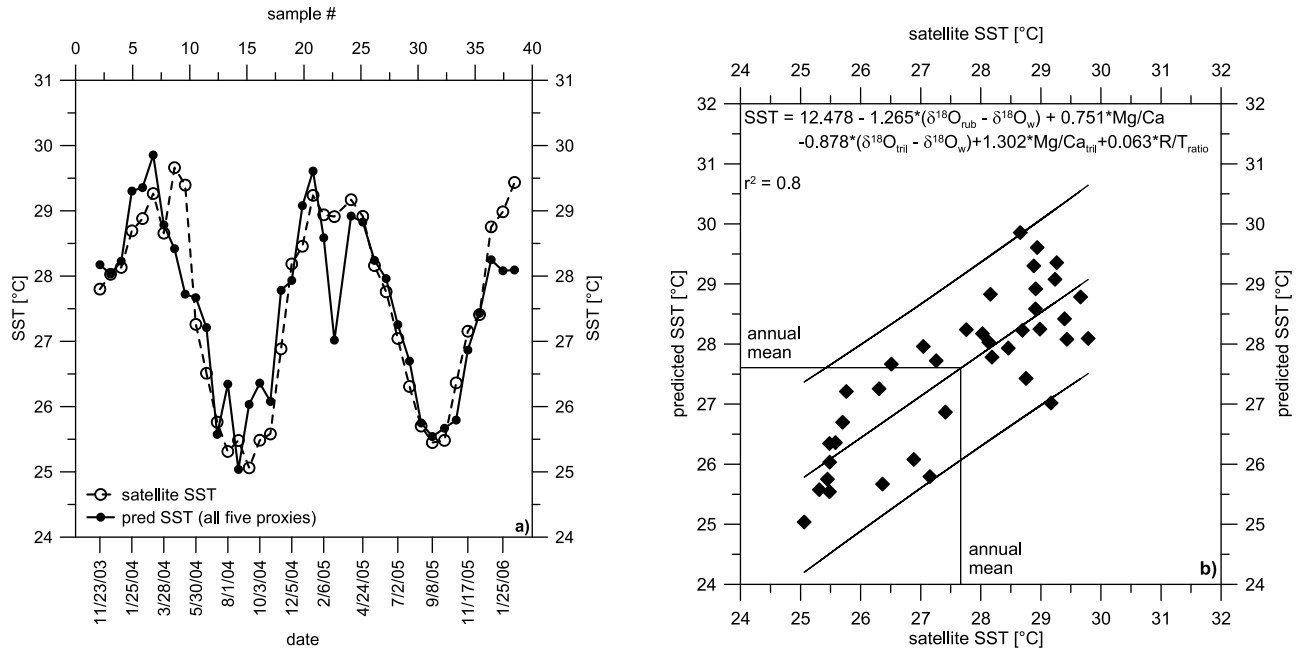

Figure 6. Observed and predicted SST calculated with calibration 6 ($\delta^{18}O_{rub}$, $\delta^{18}O_{tril}$, Mg/Ca_{rub}, Mg/Ca_{tril}, and R/T ratio) obtained from multiple linear regression. The correlation coefficient increases considerably to $r^2 = 0.80$ for all five proxies. Analysis of the residuals returns a χ^2 value of 24.00, well above the critical χ^2 of 5.99.

weighted averages for Mg/Ca also yield proxy SSTs that are 0.5°C higher (*G. ruber*) and 0.3°C lower (*G. trilobus*) than annual mean SST of 27.6°C.

[16] In order to minimize the noise in the single calibrations we applied multiple linear regression analysis to our five SST proxies (Figure 6). Multiple linear regression yields a considerably higher correlation coefficient r^2 of 0.80 than for any of the constituent proxies alone:

$$\begin{aligned} SST = {} & 12.478 - 1.265 * \left(\delta^{18}O_{rub} - \delta^{18}O_w\right) \\ & + 0.751 * Mg/Ca_{rub} - 0.878 * \left(\delta^{18}O_{tril} - \delta^{18}O_w\right) \\ & + 1.302 * Mg/Ca_{tril} + 0.063 * R/T\,\text{ratio}. \end{aligned} \quad (6)$$

Comparison of model predicted SST data (multiple regression) with satellite SST results in a better agreement between both data sets (Figure 6).

4. Discussion

[17] We have found a strong antiphase seasonality in the shell fluxes of *G. ruber* and *G. trilobus* from the Mozambique Channel in the SW Indian Ocean with *G. ruber* generating nearly half of its annual export flux in only 2 months of austral summer and *G. trilobus* in early austral winter. Despite such seasonal contrast we find flux-weighted SSTs of 28.1°C for *G. ruber* and 27.3°C for *G. trilobus* that are closer to the satellite-derived annual mean SST of 27.6°C than either summer maximum or winter minimum SSTs. Apparently, seasonal contrasts of 3.2°C are significantly dampened to 0.8°C by the relatively high shell fluxes produced during the remaining 10 months of the year with respect to minimum (*G. trilobus*) and maximum (*G. ruber*) instrumental SST of 25.0°C and 30.2°C. Flux-weighted averages show that seasonality in the Mozambique Channel only moderately affects the annual $\delta^{18}O$ and Mg/Ca temperatures given calibration errors of 0.5°C for foraminiferal paleothermometry. Rather, it provides a fine-tuning of *G. ruber* and *G. trilobus* SST calibrations that accounts for their peak anti-phase export production.

[18] We cross-correlated the $\delta^{18}O$ and Mg/Ca values of *G. ruber* and *G. trilobus* with SST in order to optimize linear regression by keeping time as the mutual constant for calibration. With respect to SST this revealed a consistent species-specific lag in their response time of 3 weeks for *G. ruber* and 6 weeks for *G. trilobus* in all proxies. Indeed, population turnover times are in the order of 2 to 4 weeks [*Bé and Hutson*, 1977; *Berger*, 1969], which defines the biological response time to SST in the (semi-) lunar domain [*Bijma et al.*, 1990; *Lončarić et al.*, 2005; *Spindler et al.*, 1979]. Shell settling experiments on *G. ruber* and *G. trilobus/sacculifer* [*Takahashi and Bé*, 1984] and field studies in high current environments [*Gyldenfeldt et al.*, 2000] indicate sinking speeds of about 400–500 m day $^{-1}$ for shells in the 250–315 μm size and 10–20 μg weight range. The time lag for our time series *G. ruber* and *G. trilobus* to settle on the 2.5 km deep ocean floor should therefore be in the order of a week. We argue that a settling time of about a week combined with 2 week population turnover time is consistent with the 3 week phase shift observed in *G. ruber* [*Bijma et al.*, 1990]. Similarly, a 1 week settling time combined with a

4 week population turnover time would account for the 6 week phase shift in *G. trilobus*.

[19] In the Mozambique Channel strong seasonality in SST is superimposed by a highly dynamic hydrography that is dominated by the intermittent passage of fast rotating mesoscale eddies through the channel [*Harlander et al.*, 2009; *Schouten et al.*, 2003]. About every 70 days, these migrating eddies strongly perturb vertical fluxes to the sediment by promoting southward expatriation of foraminifera along with their temperature proxies $\delta^{18}O$ and Mg/Ca. In addition, eddies also thoroughly mix ocean waters thereby quickly changing surface temperatures [*Donohue and Toole*, 2003]. Combined with random scatter, linear regression of the R/T ratio, $\delta^{18}O_c$, Mg/Ca against SST resulted in significant correlation, yet with relatively low coefficients. These effects can be minimized by multiple linear regression of the five independent SST proxies, that together return an r^2 of 0.80 for the SST paleothermometry in the Mozambique Channel (Figure 6).

[20] Regressions account for any species-specific offsets in $\delta^{18}O_c$ and/or Mg/Ca as a function of their differential biomineralization and also as a function of depth habitat as long as it reflects the annual SST cycle with statistically significant cross-correlations. Temperatures are constant in the surface-mixed layer (SML), the uppermost wind-mixed water column, which extends to depths between 10 and 40 m judging from the CTD profiles taken at the end of austral spring and the end of summer, consistent with modeled SML depths throughout the year (Figure 2). Indeed, the amplitudes in the seasonal $\delta^{18}O_c$ and Mg/Ca are largely similar for *G. ruber* and *G. trilobus* suggesting they experienced the same changes in temperature consistent with a similar depth habitat during the annual cycle. Both species are known surface dwellers with photosynthesizing endosymbionts that generate their export production near the bottom of the SML [*Lončarić et al.*, 2006; *Peeters and Brummer*, 2002]. For $\delta^{18}O_c$ we obtained a mean offset of 0.17‰ (Figures 4c and 4d) similar to previous observations on plankton tow samples from the Indian Ocean [*Duplessy et al.*, 1981] and for Mg/Ca of 1.2 mmol/mol (Figures 5c and 5d). The offset in Mg/Ca between both species is 0.5 mmol/mol higher than observed in other studies elsewhere [*Anand et al.*, 2003; *Huang et al.*, 2008].

[21] Offsets between *G. ruber* and *G. trilobus* in both fluxes and sediments has been variously explained in terms of differential depth habitats [*Shackleton and Vincent*, 1978; *Tedesco et al.*, 2007], pH and carbonate ion concentration [*Spero et al.*, 1997] and salinity changes [*Ferguson et al.*, 2008] contrasting in environmental settings. In SML waters of the Mozambique Channel the effects of pH, carbonate ion concentration and salinity can be considered constant with respect to foraminiferal $\delta^{18}O$ and Mg/Ca on an intra-annual time scale. While seasonal SML temperature ranges between 25 and 30.2°C, salinity remains between 34.9 and 35.3 psu and total alkalinity between 2285 and 2300 mEq/L [*Lee et al.*, 2006]. Plankton tow and calibration studies showed that *G. trilobus* usually follows the changing depth of the seasonal thermocline whereas *G. ruber* stayed in the upper 20 m [*Peeters and Brummer*, 2002; *Sadekov et al.*, 2009; *Sautter and Thunell*, 1991], yet the opposite behavior was found in the oligotrophic SE Atlantic [*Lončarić et al.*, 2007]. In the Mozambique Channel the seasonal temperature difference at 20 m and the bottom of the SML is <0.5°C as expected for the SML. We therefore argue that both *G. ruber* and *G. trilobus* were exported from near the bottom of the SML with the large and relatively constant offset between both species in $\delta^{18}O$ and Mg/Ca reflecting species-specific properties rather than different depth habitats [*Brown and Elderfield*, 1996; *Eggins et al.*, 2003].

[22] Foraminiferal SST proxies are known to be sensitive to size effects [*Elderfield et al.*, 2002; *Kroon and Darling*, 1995]. We minimized such size effects by using the very narrow size fraction of 250–315 μm for all proxies. Additionally, we analyzed how the broadening of the size fraction influences the R/T ratio. For that we counted all *G. ruber* and *G. trilobus* specimens larger than 150 μm which resulted in higher shell fluxes in winter for both species. However, this shift toward more as well as larger specimens in winter does not affect the R/T ratio which yields a similar seasonality pattern as observed for the narrow 250–315 μm fraction. We also observed that both *G. ruber* and *G. trilobus* reach maximum shell fluxes in the size fraction 250 to 350 μm as *Peeters et al.* [1999] previously showed using size-frequency distributions. This suggests that the R/T ratio has a potential as a new SST proxy.

5. Conclusions

[23] In this study we examined the first time series fluxes of planktonic foraminifera retrieved from the Mozambique Channel, upstream of the Agulhas Current. Using deep-moored sediment traps we find a distinct antiphase response to the seasonal SST fluctuation in the shell fluxes of surface-dwelling *G. ruber* and *G. trilobus*. Maximum fluxes of *G. ruber* occur in late austral summer and *G. trilobus* maxima in early winter. Despite such strong seasonality, flux-weighted $\delta^{18}O$ and Mg/Ca of both *G. ruber* and *G. trilobus* return SSTs that are close to the annual mean SST measured by satellite. Higher flux-weighted SSTs of 28.1°C (*G. ruber*) and lower flux-weighted SSTs of 27.3°C (*G. trilobus*) were observed in comparison with annual mean SST of 27.6°C. Antiphase seasonality in export fluxes accounted for the 0.8°C difference in proxy SST between summer *G. ruber* and winter *G. trilobus*, substantially lower than the mean 3.2°C seasonal contrast in instrumental SST on a 3 week basis. The ratio between shell fluxes of *G. ruber* and *G. trilobus* closely followed the seasonal cycle in SST and provides a novel proxy for regional paleothermometry upstream of the Agulhas Current. Cross-correlation of the R/T ratio, $\delta^{18}O$ and Mg/Ca of *G. ruber* and *G. trilobus* with SST yielded a conspicuous lag of 3 weeks for *G. ruber* and 6 weeks for *G. trilobus* which is consistent with their (semi-) lunar population turnover times in combination with settling velocities to the 2500 m deep ocean floor. After correcting for this lag, the first five SST calibrations are derived for the tropical SW Indian Ocean specifying flux-weighted SST. Multiple linear regression strongly improved calibration minimizing the noise associated the eddy dominated current transport found in the Mozambique Channel.

[24] **Acknowledgments.** This research was supported by the Netherlands Organization for Scientific Research (NWO) through the NEBROC, LOCO, Paleosalt (ESF-EuroClimate), SINDOCOM, and GATEWAYS programs. We thank Denise Dorhout and Wim Boer for Mg/Ca and Sr/Ca analyses as well as Michiel Kienhuis and Evaline van Weerlee for support with the mass spectrometry at the NIOZ and Suzan Verdegaal for $\delta^{18}O_w$ analyses with the Gasbench at the Free University Amsterdam. We are grateful to Jenny Ullgren for her support with statistical analyses and to Thomas Richter and Frank Peeters for their critical reading of the manuscript and discussion of the data. We thank Rainer Zahn and both anonymous reviewers for their constructive criticism that substantially improved the paper. We also acknowledge all technical support during research cruises on board the RRV *Charles Darwin*, RRV *Discovery*, and FS *Meteor*.

References

Anand, P., H. Elderfield, and M. H. Conte (2003), Calibration of Mg/Ca thermometry in planktonic foraminifera from a sediment trap time series, *Paleoceanography*, *18*(2), 1050, doi:10.1029/2002PA000846.

Barker, S., M. Greaves, and H. Elderfield (2003), A study of cleaning procedures used for foraminiferal Mg/Ca paleothermometry, *Geochem. Geophys. Geosyst.*, *4*(9), 8407, doi:10.1029/2003GC000559.

Bé, A. W. H. (1980), Gametogenic calcification in a spinose planktonic foraminifer, *Globigerinoides sacculifer* (Brady), *Mar. Micropaleontol.*, *5*(3), 283–310, doi:10.1016/0377-8398(80)90014-6.

Bé, A. W. H., and W. H. Hutson (1977), Ecology of planktonic foraminifera and biogeographic patterns of life and fossil assemblages in the Indian Ocean, *Micropaleontology*, *23*(4), 369–414, doi:10.2307/1485406.

Bé, A. W. H., D. A. Caron, and O. R. Anderson (1981), Effects of feeding frequency on life processes of the planktonic foraminifer *Globigerinoides sacculifer* in laboratory culture, *J. Mar. Biol. Assoc. U. K.*, *61*(1), 257–277, doi:10.1017/S002531540004604X.

Bemis, B. E., H. J. Spero, J. Bijma, and D. W. Lea (1998), Reevaluation of the oxygen isotopic composition of planktonic foraminifera: Experimental results and revised paleotemperature equations, *Paleoceanography*, *13*(2), 150–160, doi:10.1029/98PA00070.

Berger, W. H. (1969), Ecologic patterns of living planktonic foraminifera, *Deep Sea Res.*, *16*(1), 1–24.

Bijma, J., J. Erez, and C. Hemleben (1990), Lunar and semi-lunar reproductive cycles in some spinose planktonic foraminifers, *J. Foraminiferal Res.*, *20*(2), 117–127, doi:10.2113/gsjfr.20.2.117.

Bijma, J., and C. Hemleben (1994), Population dynamics of the planktic foraminifer *Globigerinoides sacculifer* (Brady) from the central Red Sea, *Deep Sea Res., Part I*, *41*(3), 485–510, doi:10.1016/0967-0637(94)90092-2.

Brown, S. J., and H. Elderfield (1996), Variations in Mg/Ca and Sr/Ca ratios of planktonic foraminifera caused by postdepositional dissolution: Evidence of shallow Mg-dependent dissolution, *Paleoceanography*, *11*(5), 543–551, doi:10.1029/96PA01491.

Brummer, G. J. A., C. Hemleben, and M. Spindler (1987), Ontogeny of extant spinose planktonic foraminifera (Globigerinidae): A concept exemplified by *Globigerinoides sacculifer* (Brady) and *G. ruber* (d'Orbigny), *Mar. Micropaleontol.*, *12*, 357–381, doi:10.1016/0377-8398(87)90028-4.

de Ruijter, W. P. M., A. Biastoch, S. S. Drijfhout, J. R. E. Lutjeharms, R. P. Matano, T. Pichevin, P. J. van Leeuwen, and W. Weijer (1999), Indian-Atlantic interocean exchange: Dynamics, estimation and impact, *J. Geophys. Res.*, *104*(C9), 20,885–20,910, doi:10.1029/1998JC900099.

de Ruijter, W. P. M., H. Ridderinkhof, and M. W. Schouten (2005), Variability of the southwest Indian Ocean, *Philos. Trans. R. Soc. London, Ser. A*, *363*, 63–76, doi:10.1098/rsta.2004.1478.

de Ruijter, W. P. M., G.-J. A. Brummer, S. S. Drijfhout, J. R. E. Lutjeharms, F. Peeters, H. Ridderinkhof, H. Van Aken, and P. J. van Leeuwen (2006), Observations of the interocean exchange around South Africa, *Eos Trans. AGU*, *87*(9), 97, doi:10.1029/2006EO090002.

Deuser, W. G. (1987), Seasonal variations in isotopic composition and deep-water fluxes of the tests of perennially abundant planktonic foraminifera of the Sargasso Sea—Results from sediment trap collections and their paleoceanographic significance, *J. Foraminiferal Res.*, *17*(1), 14–27, doi:10.2113/gsjfr.17.1.14.

Deuser, W. G., E. H. Ross, C. Hemleben, and M. Spindler (1981), Seasonal changes in species composition, numbers, mass, size, and isotopic composition of planktonic foraminifera settling into the deep Sargasso Sea, *Palaeogeogr. Palaeoclimatol. Palaeoecol.*, *33*(1–3), 103–127, doi:10.1016/0031-0182(81)90034-1.

Donohue, K. A., and J. M. Toole (2003), A near-synoptic survey of the southwest Indian Ocean, *Deep Sea Res., Part II*, *50*(12–13), 1893–1931, doi:10.1016/S0967-0645(03)00039-0.

Duplessy, J. C., A. W. H. Bé, and P. L. Blanc (1981), Oxygen and carbon isotopic composition and biogeographic distribution of planktonic foraminifera in the Indian Ocean, *Palaeogeogr. Palaeoclimatol. Palaeoecol.*, *33*(1–3), 9–46, doi:10.1016/0031-0182(81)90031-6.

Eggins, S., P. de Deckker, and J. Marshall (2003), Mg/Ca variation in planktonic foraminifera tests: Implications for reconstructing paleo-seawater temperature and habitat migration, *Earth Planet. Sci. Lett.*, *212*(3–4), 291–306, doi:10.1016/S0012-821X(03)00283-8.

Elderfield, H. (2002), Climate change: Carbonate mysteries, *Science*, *296*(5573), 1618–1621, doi:10.1126/science.1072079.

Elderfield, H., M. Vautravers, and M. Cooper (2002), The relationship between shell size and Mg/Ca, Sr/Ca, $\delta^{18}O$, and $\delta^{13}C$ of species of planktonic foraminifera, *Geochem. Geophys. Geosyst.*, *3*(8), 1052, doi:10.1029/2001GC000194.

Emiliani, C. (1955), Pleistocene temperatures, *J. Geol.*, *63*, 538–578, doi:10.1086/626295.

Emiliani, C., and N. J. Shackleton (1974), The Brunhes Epoch: Isotopic paleotemperatures and geochronology, *Science*, *183*(4124), 511–514, doi:10.1126/science.183.4124.511.

Erez, J., and S. Honjo (1981), Comparison of isotopic composition of planktonic foraminifera in plankton tows, sediment traps and sediments, *Palaeogeogr. Palaeoclimatol. Palaeoecol.*, *33*(1–3), 129–156, doi:10.1016/0031-0182(81)90035-3.

Fallet, U., W. Boer, C. van Assen, M. Greaves, and G.-J. A. Brummer (2009), A novel application of wet oxidation to retrieve carbonates from large organic-rich samples for ocean-climate research, *Geochem. Geophys. Geosyst.*, *10*, Q08004, doi:10.1029/2009GC002573.

Ferguson, J. E., G. M. Henderson, M. Kucera, and R. E. M. Rickaby (2008), Systematic change of foraminiferal Mg/Ca ratios across a strong salinity gradient, *Earth Planet. Sci. Lett.*, *265*(1–2), 153–166, doi:10.1016/j.epsl.2007.10.011.

Fraile, I., M. Schulz, S. Mulitza, U. Merkel, M. Prange, and A. Paul (2009), Modeling the seasonal distribution of planktonic foraminifera during the Last Glacial Maximum, *Paleoceanography*, *24*, PA2216, doi:10.1029/2008PA001686.

Greaves, M., S. Barker, C. Daunt, and H. Elderfield (2005), Accuracy, standardization, and interlaboratory calibration standards for foraminiferal Mg/Ca thermometry, *Geochem. Geophys. Geosyst.*, *6*, Q02D13, doi:10.1029/2004GC000790.

Greaves, M., et al. (2008), Interlaboratory comparison study of calibration standards for foraminiferal Mg/Ca thermometry, *Geochem. Geophys. Geosyst.*, *9*, Q08010, doi:10.1029/2008GC001974.

Gyldenfeldt, A. B., J. R. Carstens, and J. Meincke (2000), Estimation of the catchment area of a sediment trap by means of current meters and foraminiferal tests, *Deep Sea Res., Part II*, *47*(9–11), 1701–1717, doi:10.1016/S0967-0645(00)00004-7.

Harlander, U., H. Ridderinkhof, M. W. Schouten, and W. P. M. de Ruijter (2009), Long-term observations of transport, eddies, and Rossby waves in the Mozambique Channel, *J. Geophys. Res.*, *114*, C02003, doi:10.1029/2008JC004846.

Hedeker, D., and R. D. Gibbons (1996a), MIXOR: A computer program for mixed-effects ordinal regression analysis, *Comput. Methods Programs Biomed.*, *49*(2), 157–176, doi:10.1016/0169-2607(96)01720-8.

Hedeker, D., and R. D. Gibbons (1996b), MIXREG: A computer program for mixed-effects regression analysis with autocorrelated errors, *Comput. Methods Programs Biomed.*, *49*(3), 229–252, doi:10.1016/0169-2607(96)01723-3.

Huang, K.-F., C.-F. You, H.-L. Lin, and Y.-T. Shieh (2008), In situ calibration of Mg/Ca ratio in planktonic foraminiferal shell using time series sediment trap: A case study of intense dissolution artifact in the South China Sea, *Geochem. Geophys. Geosyst.*, *9*, Q04016, doi:10.1029/2007GC001660.

Kroon, D., and K. Darling (1995), Size and upwelling control of the stable isotope composition of *Neogloboquadrina dutertrei* (d'Orbigny), *Globigerinoides ruber* (d'Orbigny) and *Globigerina bulloides* (d'Orbigny): Examples from the Panama Basin and Arabian Sea, *J. Foraminiferal Res.*, *25*(1), 39–52, doi:10.2113/gsjfr.25.1.39.

Lee, K., L. T. Tong, F. J. Millero, C. L. Sabine, A. G. Dickson, C. Goyet, G.-H. Park, R. Wanninkhof, R. A. Feely, and R. M. Key (2006), Global relationships of total alkalinity with salinity and temperature in surface waters of the world's oceans, *Geophys. Res. Lett.*, *33*, L19605, doi:10.1029/2006GL027207.

Lončarić, N., G. J. A. Brummer, and D. Kroon (2005), Lunar cycles and seasonal variations in deposition fluxes of planktic foraminiferal shell carbonate to the deep South Atlantic

(central Walvis Ridge), *Deep Sea Res., Part I*, *52*(7), 1178–1188, doi:10.1016/j.dsr.2005.02.003.

Lončarić, N., F. J. C. Peeters, D. Kroon, and G.-J. A. Brummer (2006), Oxygen isotope ecology of recent planktic foraminifera at the central Walvis Ridge (SE Atlantic), *Paleoceanography*, *21*, PA3009, doi:10.1029/2005PA001207.

Lončarić, N., J. van Iperen, D. Kroon, and G. J. A. Brummer (2007), Seasonal export and sediment preservation of diatomaceous, foraminiferal and organic matter mass fluxes in a trophic gradient across the SE Atlantic, *Prog. Oceanogr.*, *73*(1), 27–59, doi:10.1016/j.pocean.2006.10.008.

Nürnberg, D., J. Bijma, and C. Hemleben (1996), Assessing the reliability of magnesium in foraminiferal calcite as a proxy for water mass temperatures, *Geochim. Cosmochim. Acta*, *60*(5), 803–814, doi:10.1016/0016-7037(95)00446-7.

Palastanga, V., P. J. van Leeuwen, and W. P. M. de Ruijter (2006), A link between low-frequency mesoscale eddy variability around Madagascar and the large-scale Indian Ocean variability, *J. Geophys. Res.*, *111*, C09029, doi:10.1029/2005JC003081.

Peeters, F. J. C., R. Acheson, G. J. A. Brummer, W. P. M. de Ruijter, R. R. Schneider, G. M. Ganssen, E. Ufkes, and D. Kroon (2004), Vigorous exchange between the Indian and Atlantic oceans at the end of the past five glacial periods, *Nature*, *430*(7000), 661–665, doi:10.1038/nature02785.

Peeters, F. J. C., and G. J. A. Brummer (2002), The seasonal distribution of living planktic foraminifera in the NW Arabian Sea, in *The Tectonic and Climatic Evolution of the Arabian Sea Region*, *J. Geol. Soc.*, *195*, 463–497.

Peeters, F. J. C., E. Ivanova, S. M. H. Conan, G. J. A. Brummer, G. M. Ganssen, S. R. Troelstra, and J. van Hinte (1999), A size analysis of planktic foraminifera from the Arabian Sea, *Mar. Micropaleontol.*, *36*(1), 31–63, doi:10.1016/S0377-8398(98)00026-7.

Rosenthal, Y., M. P. Field, and R. M. Sherrell (1999), Precise determination of element/calcium ratios in calcareous samples using sector field inductively coupled plasma mass spectrometry, *Anal. Chem.*, *71*(15), 3248–3253, doi:10.1021/ac981410x.

Rosenthal, Y., et al. (2004), Interlaboratory comparison study of Mg/Ca and Sr/Ca measurements in planktonic foraminifera for paleoceanographic research, *Geochem. Geophys. Geosyst.*, *5*, Q04D09, doi:10.1029/2003GC000650.

Sadekov, A., S. M. Eggins, P. De Deckker, U. Ninnemann, W. Kuhnt, and F. Bassinot (2009), Surface and subsurface seawater temperature reconstruction using Mg/Ca microanalysis of planktonic foraminifera *Globigerinoides ruber, Globigerinoides sacculifer*, and *Pulleniatina obliquiloculata*, *Paleoceanography*, *24*, PA3201, doi:10.1029/2008PA001664.

Sautter, L. R., and R. C. Thunell (1991), Planktonic foraminiferal response to upwelling and seasonal hydrographic conditions: Sediment trap results from San Pedro Basin, Southern California Bight, *J. Foraminiferal Res.*, *21*(4), 347–363, doi:10.2113/gsjfr.21.4.347.

Schouten, M. W., W. P. M. de Ruijter, P. J. van Leeuwen, and H. Ridderinkhof (2003), Eddies and variability in the Mozambique Channel, *Deep Sea Res., Part II*, *50*(12–13), 1987–2003, doi:10.1016/S0967-0645(03)00042-0.

Sell, D. W., and M. S. Evans (1982), A statistical analysis of subsampling and an evaluation of the Folsom plankton splitter, *Hydrobiologia*, *94*(3), 223–230, doi:10.1007/BF00016403.

Shackleton, N. J., and E. Vincent (1978), Oxygen and carbon isotope studies in recent foraminifera from the southwest Indian Ocean, *Mar. Micropaleontol.*, *3*(1), 1–13, doi:10.1016/0377-8398(78)90008-7.

Spero, H. J., J. Bijma, D. W. Lea, and B. E. Bemis (1997), Effect of seawater carbonate concentration on foraminiferal carbon and oxygen isotopes, *Nature*, *390*(6659), 497–500, doi:10.1038/37333.

Spindler, M., C. Hemleben, U. Bayer, A. W. H. Be, and O. R. Anderson (1979), Lunar periodicity of reproduction in the planktonic foraminifer *Hastigerina pelagica*, *Mar. Ecol. Prog. Ser.*, *1*(1), 61–64, doi:10.3354/meps001061.

Steinke, S., H.-Y. Chiu, P.-S. Yu, C.-C. Shen, L. Löwemark, H.-S. Mii, and M.-T. Chen (2005), Mg/Ca ratios of two *Globigerinoides ruber* (white) morphotypes: Implications for reconstructing past tropical/subtropical surface water conditions, *Geochem. Geophys. Geosyst.*, *6*, Q11005, doi:10.1029/2005GC000926.

Takahashi, K., and A. W. H. Bé (1984), Planktonic foraminifera: Factors controlling sinking speeds, *Deep Sea Res., Part A*, *31*(12), 1477–1500, doi:10.1016/0198-0149(84)90083-9.

Tedesco, K., R. C. Thunell, Y. Astor, and F. E. Müller-Karger (2007), The oxygen isotope composition of planktonic foraminifera from the Cariaco Basin, Venezuela: Seasonal and interannual variations, *Mar. Micropaleontol.*, *62*(3), 180–193, doi:10.1016/j.marmicro.2006.08.002.

van der Werf, P. M., P. J. van Leeuwen, H. Ridderinkhof, and W. P. M. de Ruijter (2010), Comparison between observations and models of the Mozambique Channel transport: Seasonal cycle and eddy frequencies, *J. Geophys. Res.*, *115*, C02002, doi:10.1029/2009JC005633.

G.-J. Brummer, U. Fallet, S. Vogels, and J. Zinke, Department of Marine Geology, Royal NIOZ, PO Box 59, NL-1790 AB Den Burg, Netherlands. (geert-jan.brummer@nioz.nl; ulrike.fallet@nioz.nl; sanne.vogels@falw.vu.nl; jens.zinke@nioz.nl)

H. Ridderinkhof, Department of Physical Oceanography, Royal NIOZ, PO Box 59, NL-1790 AB Den Burg, Netherlands. (herman.ridderinkhof@nioz.nl)